Multifunctional Cyanine-Based Theranostic Probe

Subjects: Radiology, Nuclear Medicine & Medical Imaging

Contributor: Cheng-Liang Peng

Cancer is one of the leading causes of death in the world. A cancer-targeted multifunctional probe labeled with the radionuclide has been developed to provide multi-modalities for NIR fluorescence and nuclear imaging (PET, SPECT), for photothermal therapy (PTT), and targeted radionuclide therapy of cancer. In this entry, researchers synthetized a cancer-targeted multimodal probe (DOTA-NIR790 as shown in Figure 1) for cancer imaging and therapy by the mitochondrial potential difference between cancers and the surrounding normal tissues.

Keywords: multi-modality ; cyanine dye ; near-infrared fluorescence imaging ; nuclear imaging ; photothermal therapy ; targeted radionuclide therapy

1. Introduction

Early cancer detection represents the most promising way to reduce the growth of cancer [1]. Additionally, about 1000 million people worldwide suffer from cancer every year, with an increase number of people with cancer around the world, the development of drugs for cancer diagnosis and treatment is an important part of the biological medicine. The most common form of cancer is a solid tumor of the lung, breast, prostate, colon, and rectum. If the cancer can be diagnosed at an early stage, most cancer patients after surgery, radiotherapy, chemotherapy, or combination therapy can survival for a long time. The five-year survival rate of for early-stage cancer is up to 90%.

Therefore, accurate early detection makes it possible to perform all kinds of treatment prior to tumor progression. The cancer currently can be detected by many imaging modalities, including computed tomography (CT), single-photon emission computed tomography (SPECT), positron emission tomography (PET), ultrasonography, and magnetic resonance imaging (MRI) [2]. However, there are still many significant challenges in using molecular imaging for cancer detection, including that most of the specific receptors are not overexpressed in all types of cancer. Therefore, the development of a versatile molecular probe to detect the majority of cancer tissue has considerable benefits.

Near infrared fluorescent heptamethine cyanine dyes including indocyanine green (ICG), IR-783 and IR-780 iodide, has been shown to have abilities for noninvasive tumor imaging [3][4][5]. It was reported that cancer cells have higher mitochondrial membrane potential (ΔΨm) than normal cells [6] Because of mitochondrial membrane potential (ΔΨm) alteration in cancer cells, delocalized cationic compounds could accumulate in the hyperpolarized mitochondria as a tumor-targeting agent for imaging and therapy [7][8][9]. For example, rhodamine-123, Acridinium, and cyanine dyes have been used for in vitro and in vivo fluorescent imaging of the altered mitochondrial membrane potential in tumor cells, and as radiotracers for nuclear imaging of tumors [6][10][11][12]. In addition, several radiolabeled triphenylphosphonium (TPP) cations were used as radiotracers for nuclear tumor imaging [13][14].

For the treatment of primary or metastatic tumors, although surgical resection is the standard treatment, the tumors are not easy to remove by surgery in many situations. Therefore, imaging-guided cancer surgery will offer more effective and safe modalities of cancer therapy [15]. When the tumor in patients are really not suitable for surgery, tumor thermal ablation is another low-invasive treatment modality [16]. Photothermal therapy (PTT) destroys cancer cells by generating heat within a tumor by absorbing specific light sources [17][18]. The heptamethine cyanine dyes also exhibits unique optical properties due to its strong absorption at NIR wavelengths, which causes photothermal effects that can trigger thermal injury and cell death both in vitro and in vivo [6][7][8][9].

Indium-111 (^{111}In, half-life = 2.83 days) only emits γ-ray (23, 171 and 245 keV), and is commonly used in nuclear imaging by radiolabeling targeted molecules [19]. In this study, Indium-111 was used as a diagnostic radionuclide to label with DOTA-NIR790 for nuclear imaging of cancers. Lutetium-177 (^{177}Lu, half-life = 6.73 days) is an emerging, promising medium-energy beta-emitter (490 keV) with a low-abundance gamma emission (208 keV, 11% abundance) for biomedical use. This unique property makes ^{177}Lu as a suitable radionuclide candidate for both therapeutic and diagnostic purposes.

In this study, researchers synthetized a cancer-targeted multimodal probe (DOTA-NIR790 as shown in **Figure 1**) for cancer imaging and therapy by the mitochondrial potential difference between cancers and the surrounding normal tissues. Compared with other reported cyanine-based theranostic probes, the DOTA-NIR790 has the additional chelated capabilities of radioisotope for nuclear imaging and targeted radionuclide therapy of cancers. DOTA-NIR790 is a single molecule with multi-functions for cyanine-based near-infrared fluorescence imaging and photothermal therapy of cancers, and for nuclear imaging and targeted radionuclide therapy of cancers after radioisotope-labeling. The heptamethine cyanine-based dye allowed the DOTA-NIR790 to have dual functions in cancer NIR imaging and photothermal therapy (PTT). The DOTA-NIR790 will be labeled with lutetium-177 to detect tumors by using SPECT imaging and kill cancer cells by its beta-emission. The ^{177}Lu-DOTA-NIR790 enabled imaging by NIR fluorescence and by nuclear imaging (SPECT) to monitor in real-time the tumor accumulation, intra-tumoral distribution, and the situation of cancer therapy, and to guide the surgery or the photothermal therapy of the cancer.

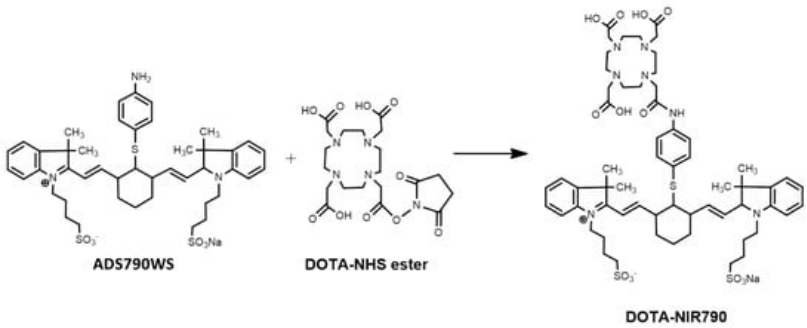

Figure 1. Synthesis of DOTA-NIR790.

2. Characterization of DOTA-NIR790 and Radionuclide-Labeled DOTA-NIR790

The obtained crude product was purified by preparative HPLC as shown in the Supplementary Materials, Figure S1A. The collected DOTA-NIR790 (R_t = 9.2 min) was frozen and lyophilized overnight. Finally, the pure product was collected with a yield of 17.2%, and its chemical purity was more than 95%. The mass spectrometry and ^{1}H-NMR spectrum analysis were shown in the Supplementary Materials, Figure S1B,C. As shown in Figure S2, the radiochemical purity of ^{111}In-DOTA-NIR790 was more than 95% by radio-HPLC analysis, and the radiochemical purity of ^{177}Lu-DOTA-NIR790 was more than 90% by ITLC.

3. Cellular Uptake of ^{111}In-DOTA-NIR790

In this experiment, CCCP was used to disrupt the mitochondrial potential in various cancer cells, resulting in inhibition on cellular uptake of ^{111}In-DOTA-NIR790. **Figure 2** illustrates representative uptake of the cancer cells treated with ^{111}In-DOTA-NIR790 with/without CCCP. It is quite clear that the cellular uptake of ^{111}In-DOTA-NIR790 was dose-dependently decreased by CCCP. It demonstrated that In-111-DOTA-NIR790 accumulates in cancer cells through mitochondrial membrane potential (ΔΨm) alteration.

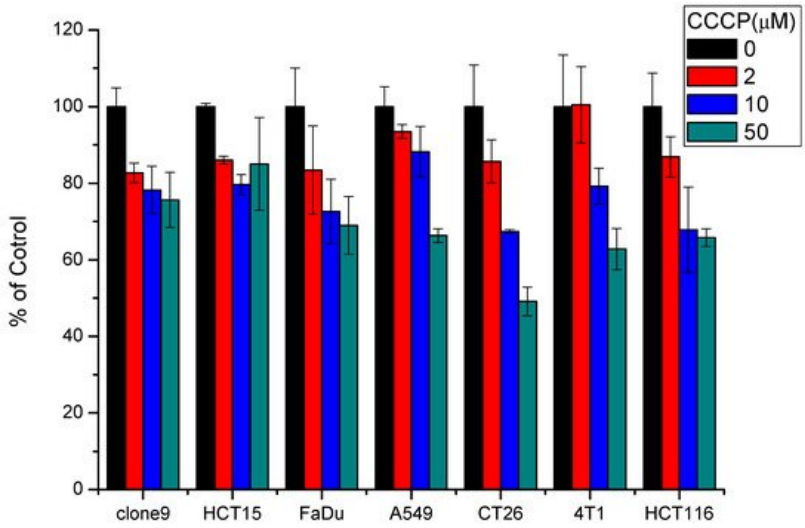

Figure 2. Representative uptake of ^{111}In-DOTA-NIR790 in various cancer cells treated with 0, 2, 10, and 50 μM of carbonyl cyanine m-chlorophenylhydrazone (CCCP) (*n* = 3 per concentration of CCCP and cell).

4. Biodistribution of ^{111}In-DOTA-NIR790 in Mice Bearing Subcutaneous 4T1 Tumors

This experiment was performed by single photon computed tomography (SPECT) and near infrared fluorescence imaging (NIRF). The biodistribution of multi-functional probes ^{111}In-DOTA-NIR790 in mice bearing subcutaneous tumors was evaluated. First, ^{111}In-DOTA-NIR790 (~37 MBq) were intravenously injected into mice with subcutaneous 4T1 breast tumor, and imaged on a SPECT/CT at 1, 4, 24, and 48 h, as shown in **Figure 3**a. Then, the mice were sacrificed and the organs were collected for quantitative analysis by gamma-counter, as shown in **Figure 3**b. According to the biodistribution, the ^{111}In-DOTA-NIR790 has a much larger accumulation amount at the tumor site than the muscle tissue with the tumor/muscle ratio of 12.84 ± 0.65 at 48 h. It is mainly due to the fact that the hydrophilic ^{111}In-DOTA-NIR790 can be cleared from normal tissues and organs more quickly, which can cause ^{111}In-DOTA-NIR790 to have better tumor contrast and lower side effects in future applications of therapeutic isotopes. The NIRF imaging of mice bearing tumors was received at 1, 4, 24, and 48 h after intravenous injection of ^{111}In-DOTA-NIR790 by the IVIS imaging system. The results are shown in **Figure 3**c. The mice were sacrificed and the organs were collected for the ex vivo NIRF imaging of organs and tumor and quantitative analysis of fluorescence intensity at 48 h after injection of ^{111}In-DOTA-NIR790 as shown in Supplementary materials, Figure S3.

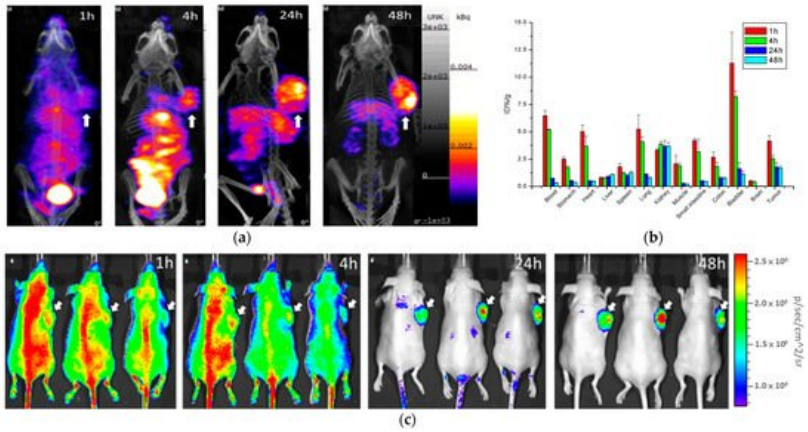

Figure 3. (**a**) SPECT/CT images, (**b**) biodistribution, and (**c**) NIRF images of ^{111}In-DOTA-NIR790 in mice bearing subcutaneous 4T1 breast tumors (*n* = 3 at each time point). Arrow indicates tumor.

5. Biodistribution of ^{111}In-DOTA-NIR790 in Mice with Brain Metastasis of Breast Cancer

^{111}In-DOTA-NIR790 (about 37MBq of In-111) was intravenously injected into mice with brain metastasis of 4T1 breast cancer, and the NanoSPECT/CT imaging of the brain was performed at 48 h after administration as shown in **Figure 4**a. In addition, the IVIS imaging system was used for near-infrared fluorescence imaging of ^{111}In-DOTA-NIR790 at 48 h after administration as shown in **Figure 4**b. After the mice were sacrificed, their brain tissues were extracted and quantitatively analyzed by gamma-counter at 24 and 48 h after injection, as shown in **Figure 4**c. The ex vivo NIRF images of brains with metastatic 4T1 breast cancer were shown in **Figure 4**d. According to these results, this probe can specifically bind to brain metastasis of 4T1 breast tumor, and similar results are obtained in SPECT and near-infrared light imaging.

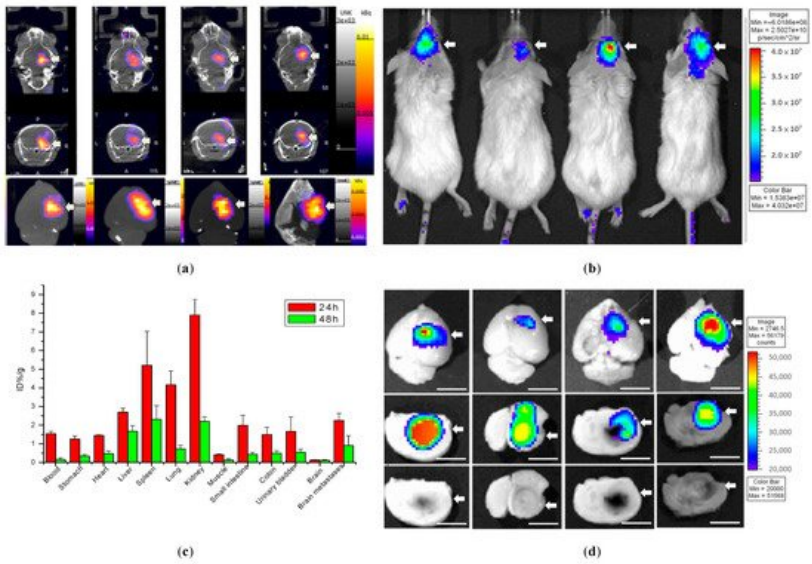

Figure 4. Biodistribution of ^{111}In-DOTA-NIR790 in mice with brain metastasis of 4T1 breast cancer. (**a**) SPECT/CT images, (**b**) NIRF images, (**c**) biodistribution, and (**d**) ex vivo NIRF images at 48 h after administration (*n* = 4 at each time point). Arrow indicates tumor. The scale bar is 5 mm.

6. Biodistribution of ^{111}In-DOTA-NIR790 in Mice with Subcutaneous Colon Cancer and Lung Cancer

Figure 5 shows the single-photon computed tomography (SPECT) images and biodistribution results of the multi-function probe ^{111}In-DOTA-NIR790 in mice bearing CT-26 tumor at 1, 4, 24, 48 h post-injection. The amount of tumor accumulation was 5.39 ± 0.40% and 3.19 ± 0.49% ID/g at 24 h and 48 h, respectively, and the tumor-to-muscle accumulation ratio was 15.18 ± 2.13 at 48 h. In **Figure 6**, the results of the SPECT images and biodistribution of ^{111}In-DOTA-NIR790 in the mouse model of human lung cancer A549 showed that the amount of tumor accumulation was 2.65 ± 0.21% and 2.31 ± 0.15% ID/g at 24 and 48 h, respectively. The tumor to muscle accumulation ratio at the 48th hour was 18.98 ± 3.35. The tumor/muscle ratios in mouse model of various cancers are summarized as shown in **Table 1**.

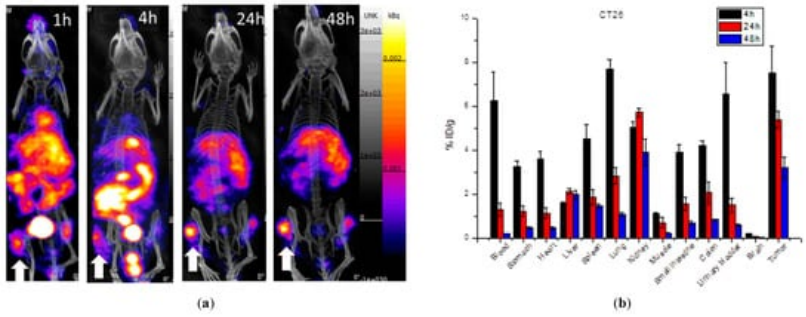

Figure 5. (**a**) SPECT/CT images and (**b**) biodistribution of ^{111}In-DOTA-NIR790 in mice bearing subcutaneous CT-26 colon cancer (*n* = 3 at each time point). Arrow indicates tumor.

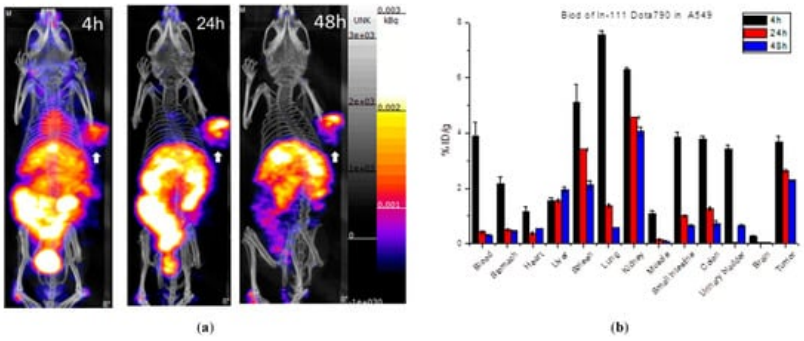

Figure 6. (**a**) SPECT/CT images and (**b**) biodistribution of ^{111}In-DOTA-NIR790 in mice bearing subcutaneous A549 lung cancer (*n* = 3 at each time point). Arrow indicates tumor.

Table 1. Tumor/Muscle Ratio of ^{111}In-DOTA-NIR790 in various cancer at 48 h after administration.

Cancer Model	Tumor/Muscle Ratio
4T1 breast cancer	12.84 ± 0.65
CT26 colon cancer	15.18 ± 2.13
A549 lung cancer	18.98 ± 3.35

7. Anti-Tumor Efficacy of ^{177}Lu-DOTA-NIR790 with NIR Irradiation

To evaluate the effect of DOTA-NIR790 on photothermal therapy of cancer, the results were shown in **Figure 7**. After exposure to laser light at 808 nm (1.8 w/cm^2), the tumor temperature during irradiation was measured by thermal camera. The infrared thermographic map showed that the tumor temperature was effectively increased to about 48.6 °C after 5 min of irradiation, when the mice treated with 15 mg/kg of DOTA-NIR790.

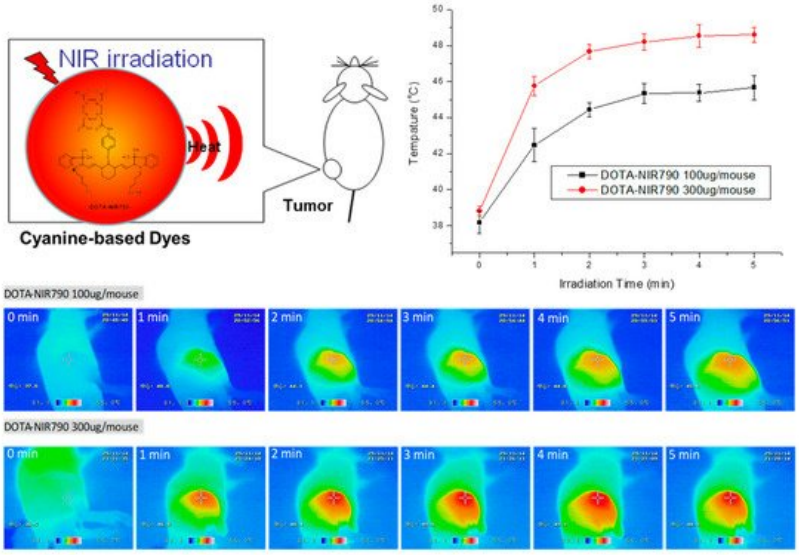

Figure 7. Tumor temperature measurement (*n* = 3 at each time point) and infrared thermographic map during irradiation of DOTA-NIR790 based photothermal therapy.

As shown in **Figure 8**A, mice were treated with DOTA-NIR790, the tumor growth was effectively inhibited by laser irradiation, compared to the control group. The results of tumor growth inhibition also show that the tumor temperature caused by the photothermal effect of DOTA-NIR790 is elevated, which can effectively ablate the tumor and cause scarring of the tumor tissue at the illumination site. In addition, the experimental results show that photothermal therapy alone or targeted radionuclide therapy alone by ^{177}Lu-DOTA-NIR790, has significant tumor growth inhibition compared with the control group. The combination of photothermal therapy and targeted radionuclide therapy by ^{177}Lu-DOTA-NIR790 has an additive effect in tumor growth inhibition. Body weight loss was used as a measure of treatments-induced toxicity (**Figure 8**B). Representative mice treated with ^{177}Lu-DOTA-NIR790 and NIR irradiation for 5 min were photographed as shown in **Figure 8**C. Scabs of tumor thermal ablation were observed on the flanks of mice after DOTA-NIR790-based photothermal therapy.

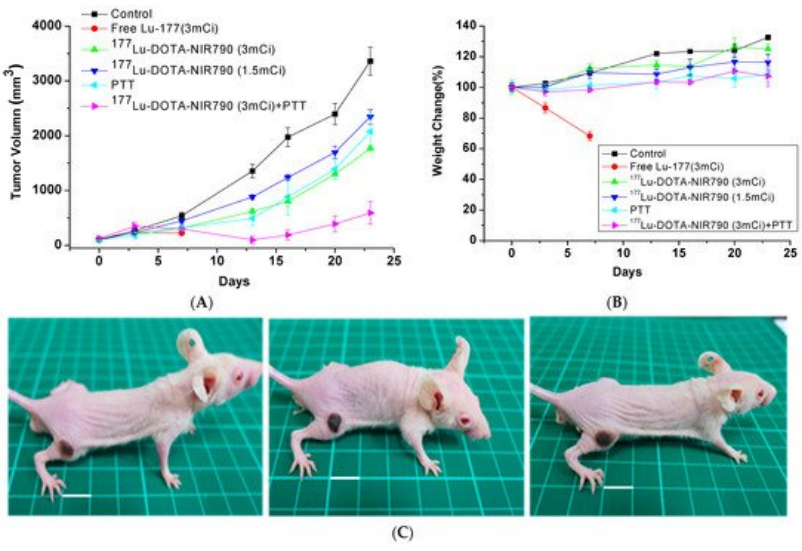

Figure 8. Anti-tumor effect of multi-functional tumor theranostics probes. (**A**) Tumor growth inhibition of photothermal therapy (PTT) combined with targeted radionuclide therapy by ^{177}Lu-DOTA-NIR790 (n = 6 per group) (**B**) body weight changes, and (**C**) Representative mice treated with ^{177}Lu-DOTA-NIR790 and NIR irradiation for 5 min were photographed. The scale bar is 10 mm.

The body weights of both control and treatment groups were monitored throughout the experimental period. Mice treated with 111 MBq of Lu-177 lost over 30% of their weight and died at day 7. The control groups treated with PBS or targeted radionuclide therapy by ^{177}Lu-DOTA-NIR790 gradually had increased their body weights by 17~30%. These values were not significantly different between each treatment, which suggested that the dose of ^{177}Lu-DOTA-NIR790 was reasonably well-tolerated. Mice treated with combination of photothermal therapy and targeted radionuclide therapy by ^{177}Lu-DOTA-NIR790 increased 5% of their weight at day 24. This weight change was not significantly different from other single treatment, indicating that combination of photothermal therapy and targeted radionuclide therapy mediated by ^{177}Lu-DOTA-NIR790 did not result in unacceptable toxicity.

As shown in **Figure 9**, the histopathological and immunohistochemical analysis showed that DOTA-NIR790-mediated photothermal therapy can cause necrosis and vacuolation in the internal tissues of the tumor, inhibit the ability of tumor cell replication (decreased expression of PCNA), and the high expression of HSP protein revealed that the tumor tissue received thermal shock by the photothermal therapy.

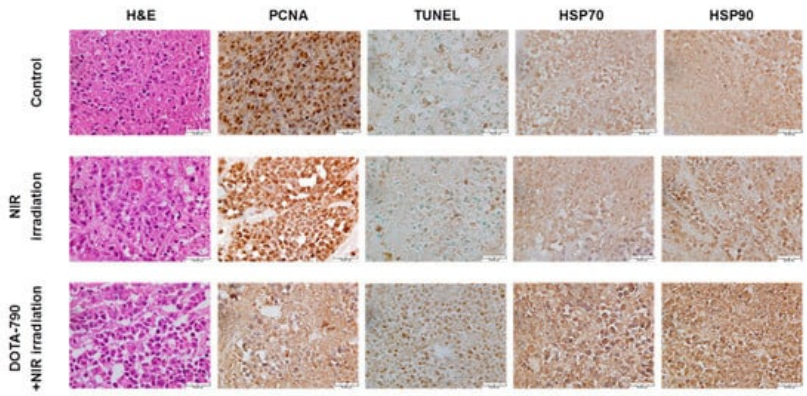

Figure 9. Histological and immunohistochemical analysis in 4T1 tumors treated with DOTA-NIR790-mediated photothermal therapy. The scale bar is 50 μm.

References

1. Etzioni, R.; Urban, N.; Ramsey, S.; McIntosh, M.; Schwartz, S.; Reid, B.; Radich, J.; Anderson, G.; Hartwell, L. The case for early detection. Nat. Rev. Cancer 2003, 3, 243–252.
2. Kircher, M.F.; Willmann, J.K. Molecular Body Imaging: MR Imaging, CT, and US. Part I. Principles. Radiology 2012, 263, 633–643.
3. Rao, J.H.; Dragulescu-Andrasi, A.; Yao, H.Q. Fluorescence imaging in vivo: Recent advances. Curr. Opin. Biotechnol. 2007, 18, 17–25.
4. Yang, X.J.; Shi, C.M.; Tong, R.; Qian, W.P.; Zhau, H.E.; Wang, R.X.; Zhu, G.D.; Cheng, J.J.; Yang, V.W.; Cheng, T.M.; et al. Near IR Heptamethine Cyanine Dye-Mediated Cancer Imaging. Clin. Cancer Res. 2010, 16, 2833–2844.
5. Zhang, C.; Liu, T.; Su, Y.; Luo, S.; Zhu, Y.; Tan, X.; Fan, S.; Zhang, L.; Zhou, Y.; Cheng, T.; et al. A near-infrared fluorescent heptamethine indocyanine dye with preferential tumor accumulation for in vivo imaging. Biomaterials 2010, 31, 6612–6617.
6. Zhou, Y.; Kim, Y.-S.; Yan, X.; Jacobson, O.; Chen, X.; Liu, S. 64Cu-Labeled Lissamine Rhodamine B: A Promising PET Radiotracer Targeting Tumor Mitochondria. Mol. Pharm. 2011, 8, 1198–1208.
7. Modica-Napolitano, J.S.; Aprille, J.R. Delocalized lipophilic cations selectively target the mitochondria of carcinoma cells. Adv. Drug Deliv. Rev. 2001, 49, 63–70.
8. Zhou, Y.; Liu, S. 64Cu-Labeled Phosphonium Cations as PET Radiotracers for Tumor Imaging. Bioconjugate Chem. 2011, 22, 1459–1472.
9. Licha, K.; Olbrich, C. Optical imaging in drug discovery and diagnostic applications. Adv. Drug Deliv. Rev. 2005, 57, 1087–1108.

10. Zhou, Y.; Kim, Y.-S.; Shi, J.; Jacobson, O.; Chen, X.; Liu, S. Evaluation of 64Cu-Labeled Acridinium Cation: A PET Radiotracer Targeting Tumor Mitochondria. Bioconjugate Chem. 2011, 22, 700–708.
11. Xiao, L.; Zhang, Y.; Yue, W.; Xie, X.; Wang, J.-p.; Chordia, M.D.; Chung, L.W.K.; Pan, D. Heptamethine cyanine based 64Cu-PET probe PC-1001 for cancer imaging: Synthesis and in vivo evaluation. Nucl. Med. Biol. 2013, 40, 351–360.
12. Onoe, S.; Temma, T.; Shimizu, Y.; Ono, M.; Saji, H. Investigation of cyanine dyes for in vivo optical imaging of altered mitochondrial membrane potential in tumors. Cancer Med. 2014, 3, 775–786.
13. Steichen, J.D.; Weiss, M.J.; Elmaleh, D.R.; Martuza, R.L. Enhanced in vitro uptake and retention of 3H-tetraphenylphosphonium by nervous system tumor cells. J. Neurosurg. 1991, 74, 116–122.
14. Min, J.-J.; Biswal, S.; Deroose, C.; Gambhir, S.S. Tetraphenylphosphonium as a Novel Molecular Probe for Imaging Tumors. J. Nucl. Med. 2004, 45, 636–643.
15. 15 Chi, C.; Du, Y.; Ye, J.; Kou, D.; Qiu, J.; Wang, J.; Tian, J.; Chen, X. Intraoperative Imaging-Guided Cancer Surgery: From Current Fluorescence Molecular Imaging Methods to Future Multi-Modality Imaging Technology. Theranostics 2014, 4, 1072–1084.
16. Rahbari, N.N.; Mehrabi, A.; Mollberg, N.M.; Muller, S.A.; Koch, M.; Buchler, M.W.; Weitz, J. Hepatocellular Carcinoma Current Management and Perspectives for the Future. Ann. Surg. 2011, 253, 453–469.
17. Hirsch, L.R.; Stafford, R.J.; Bankson, J.A.; Sershen, S.R.; Rivera, B.; Price, R.E.; Hazle, J.D.; Halas, N.J.; West, J.L. Nanoshell-mediated near-infrared thermal therapy of tumors under magnetic resonance guidance. Proc. Natl. Acad. Sci. USA 2003, 100, 13549–13554.
18. Gobin, A.M.; Lee, M.H.; Halas, N.J.; James, W.D.; Drezek, R.A.; West, J.L. Near-Infrared Resonant Nanoshells for Combined Optical Imaging and Photothermal Cancer Therapy. Nano Lett. 2007, 7, 1929–1934.
19. Bhattacharyya, S.; Dixit, M. Metallic radionuclides in the development of diagnostic and therapeutic radiopharmaceuticals. Dalton Trans. 2011, 40, 6112–6128.

Retrieved from https://encyclopedia.pub/entry/history/show/39248